Supplement of Hydrol. Earth Syst. Sci., 30, 3789–3804, 2026
https://doi.org/10.5194/hess-30-3789-2026-supplement

Hydrology and Earth System Sciences
Open Access
EGU

Supplement of

From salinity to nanoplastics: redefining safe yield in strip-island aquifers under emerging contaminant threats

Tianyuan Zheng et al.

Correspondence to: Tianyuan Zheng (zhengtianyuan@ouc.edu.cn) and Shaobo Gao (gaoshaobo@ouc.edu.cn)

Content

S1. Groundwater flow equations for the unsaturated zone and salinity transport equations.....2

S2. Synthesis of Hydrophilic and Hydrophobic nanoplastics 3

S3. Column Experiment 4

S4. Comparison of the Migration Capabilities of Hydrophilic and Hydrophobic Nanoplastics 5

S1. Groundwater flow equations for the unsaturated zone and salinity transport equations

The governing equation for variable-density groundwater flow in the unsaturated-saturated zone is given by the Richards equation:

$$\theta\rho\frac{\partial S_{\mathrm{W}}}{\partial t}+\theta S_{\mathrm{W}}\frac{\partial\rho}{\partial C}\frac{\partial C}{\partial t}=\nabla\cdot\rho\left(\frac{k_{\mathrm{r}}\mathbf{k}}{\mu}\left(\nabla P+\rho g\nabla Z\right)\right)+\rho q_{\mathrm{ss}} \tag{S1}$$

where θ is the porosity [-], ρ is the fluid density [ML−3], S_{W} is the saturation [-], C is the salt concentration of the fluid [ML^{-3}], $\mathbf{k}$ is the saturated permeability coefficient [LT^{-1}], k_{r} is the relative permeability coefficient [-], μ is the dynamic viscosity [ML-1T-1], P is fluid pressure, varying with time [$ML^{-1}T^{-2}$], g is the gravitational acceleration [LT^{-2}]; Z is elevation[L], q_{ss} is the source-sink term [T^{-1}].

The solute transport equation, describing advective and dispersive salt migration in groundwater, conserves solute mass as follows:

$$\frac{\partial S_{\mathrm{W}}\theta C}{\partial t}=\nabla\cdot\rho\left[S_{\mathrm{W}}D\nabla\left(\frac{C}{\rho}\right)\right]+\nabla\cdot C\frac{k_{\mathrm{r}}\mathbf{k}}{\mu}\nabla P+q_{\mathrm{ss}}C_{\mathrm{ss}} \tag{S2}$$

where D is the hydrodynamic dispersion coefficient [L^2T^{-1}], and C_{ss} is the salt concentration of the source-sink term [ML^{-3}].

The relationship between relative permeability, capillary pressure, and phase saturation in unsaturated aquifers is described by the van Genuchten curve (van Genuchten et al., 1980):

$$S_{\mathrm{w}}=S_{\mathrm{res}}+\left(1-S_{\mathrm{res}}\right)\left(\frac{1}{1+\left(a|\psi|\right)^{n}}\right)^{\frac{n-1}{n}} \tag{S3}$$

$$k_{\mathrm{r}}=S_{\mathrm{e}}^{l}\left\{1-\left[1-S_{\mathrm{e}}^{n/(n-1)}\right]^{(n-1)/n}\right\}^{2} \tag{S4}$$

$$S_{\mathrm{e}}=\frac{S_{\mathrm{w}}-S_{\mathrm{res}}}{1-S_{\mathrm{res}}} \tag{S5}$$

where S_{res} is the residual water saturation [-], a, n and l is the corresponding constants [-], S_{e} is the effective water saturation [-].

S2. Synthesis of Hydrophilic and Hydrophobic nanoplastics

Poly(styrene) nanoparticles loaded with palladium (PS-Pd NPs) were synthesised via a two-step emulsion polymerisation method, comprising core formation and shell construction stages. First, 12.0 g of acrylonitrile (AN), 0.36 g of sodium dodecyl sulphate (SDS), and 0.36 g of potassium perpolysulphate (KPS) were added to a reaction vessel containing 108.0 g of deionised water (60°C). The mixture was stirred at 300 rpm until complete dissolution. Continuous nitrogen gas was introduced to eliminate oxygen from the reaction system. Subsequently, 0.24 g of potassium polyethylene glycol 4-nonylphenyl 3-sulfonylpropyl ether (KPE) and 0.18 g of K_2PdCl_4, each dissolved in 8.0 mL of deionised water, were added to the reaction vessel via syringe over 2 minutes. The mixture reacted at 60°C for 40 minutes to form the polymer core.

Whilst the core reaction proceeds continuously, the monomer composition within the reaction system is gradually modulated via two peristaltic pumps and two feeders (Feeder 1 and Feeder 2), thereby achieving the transition from the AN core to the styrene shell. Feeder 1 was supplemented with styrene, AN, and deionised water; Feeder 2 contained styrene, SDS, divinylbenzene (DVB), and deionised water. The specific quantities of reagents used in the synthesis of PS-Pd-1 and PS-Pd-2 are listed in Table S1. Additionally, an appropriate amount of KPS (PS-Pd-1: 0.18 g; PS-Pd-2: 0.09 g) was dissolved in 4.0 g of deionised water and directly injected into the reaction vessel.

Activate the peristaltic pump (flow rate 0.02 mL/min) to transfer the solution from Feeder 2 into Feeder 1, and subsequently from Feeder 1 into the reaction vessel. This process shall continue for 2 hours. Thereafter, remove Feeder 1 and directly inject the solution from Feeder 2 into the reaction system, allowing the reaction to proceed for a further 0.5 hours. Following removal of Feeder 2, the reaction mixture shall continue to react within the vessel for an additional 2 hours. Finally, add 20.0 g of deionised water and react for 10 minutes to terminate the polymerisation.

Upon completion of the reaction, remove the vessel from the oil bath. Centrifuge the resulting product five times with ethanol (5000 rpm, 10 minutes per run). Place the centrifuged precipitate in deionised water for dialysis over three days, replacing the dialysis buffer daily. All reagents used in the experiment were purchased from Sigma Aldrich.

S3. Column Experiment

Column experiments were conducted according to previously reported methodologies for studying nanoplastics migration in sediments, with the experimental apparatus schematic shown in Figure 1. The packed column was first pre-equilibrated using deionised water, followed by the injection of 20 column volumes (PV) of artificial seawater as background solution at a flow rate of 4.0 mL/min. Subsequently, 5 PV of a 10 mg/L nanoplastic suspension was injected at the same flow rate, followed by elution with an additional 5 PV of seawater. To prevent sedimentation of nanoplastic particles, the suspension was continuously homogenised during injection via a magnetic stirrer.

During the migration experiment, effluent samples were collected every 10 minutes. The concentration of palladium (Pd) in these samples was determined using inductively coupled plasma mass spectrometry (ICP-MS). Based on this, quantitative calibration curves for the concentrations of PS-Pd-1 and PS-Pd-2 nanoplastics in seawater were established, enabling quantitative analysis of the migration behaviour of the nanoplastics. By adjusting the parameters, the simulation results achieved high consistency with the experimental results in the breakthrough curve.($R^2 > 9.0$)

S4. Comparison of the Migration Capabilities of Hydrophilic and Hydrophobic Nanoplastics

Laboratory-scale deep extraction simulations revealed distinct spatiotemporal distribution differences between hydrophilic (PS-Pd-1) and hydrophobic (PS-Pd-2) nanoplastics (NPs) during the initial stress period, with such variations governed by the intrinsic surface properties of NPs that modulate their adsorption interactions with aquifer solid media. The initial spatial distributions of the two MP types (Fig. S5(a_1, b_1)) characterize the occurrence pattern of NPs in groundwater subsequent to freshwater lens formation, while their temporal evolution profiles (Fig. S5(a_2-a_4), (b_2-b_4)) demonstrate a rapid expansion of the PS-Pd-2 plume, verifying its superior mobility—this is attributed to weak electrostatic and van der Waals forces between hydrophobic PS-Pd-2 and aquifer solids, which minimize particulate retention and facilitate advective transport. Notably, the contamination area of PS-Pd-2 reached 29.6% under initial conditions, exactly twice that of PS-Pd-1 (14.8%). Under pumping conditions, their distribution patterns showed significant divergence: PS-Pd-1 and PS-Pd-2 covered 17.1% and 43.5% of the reconfigured freshwater lens area, respectively. Hydrophobic PS-Pd-2 presented broader liquid-phase retention in the freshwater lens due to its stronger dispersion properties, whereas hydrophilic PS-Pd-1 exhibited enhanced solid-phase adsorption driven by its high surface energy, resulting in pronounced solid-phase accumulation and a reduced fraction in the mobile aqueous phase. MP concentrations decreased by approximately 50% on average in the central lens region below the mid-lens area, with no such attenuation in the high-flow seawater exchange zones on both sides, where intensified advective transport counteracts the reduction of MP concentrations.

Hydrophobic PS-Pd-2 consistently exhibited a more extensive spatial distribution and a stronger accumulation tendency in the groundwater system during pumping (Fig. S5), a phenomenon synergistically induced by its inherent physicochemical properties and pumping-triggered hydrodynamic perturbations. Its low surface hydrophilicity weakens solid-phase retention, sustaining high mobility in the aqueous phase, while the radial flow generated by pumping further drives the migration and enrichment of PS-Pd-2 toward the pumping well. During pumping operations, the 1% C_{nps} isoconcentration line of hydrophobic NPs exceeded the wellhead within 3 minutes, whereas that of hydrophilic NPs never reached the well height at any time, as PS-Pd-1 was immobilized by irreversible solid-phase adsorption onto aquifer media. Notably, the freshwater lens contracted rapidly and reached stability within 3 minutes in simulations with hydrophilic NPs; this accelerated contraction originated from the solid-phase adsorption of PS-Pd-1, which caused pore blockage in the aquifer, altered its hydraulic conductivity, and thus inhibited groundwater recharge to the lens. The environmental hazards of

hydrophobic NPs stem not only from their physical impacts as particulate matter but also from their role as efficient toxicant carriers—their low surface free energy enables the adsorption, concentration and subsequent release of various toxic chemicals in biological organisms, inducing combined toxic effects.

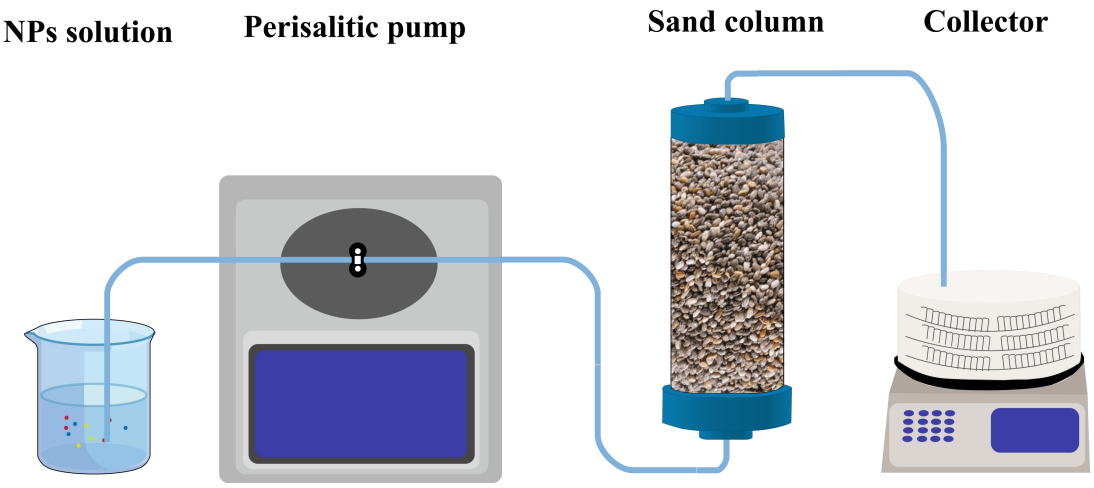

Figure. S1. Column Experiment Apparatus

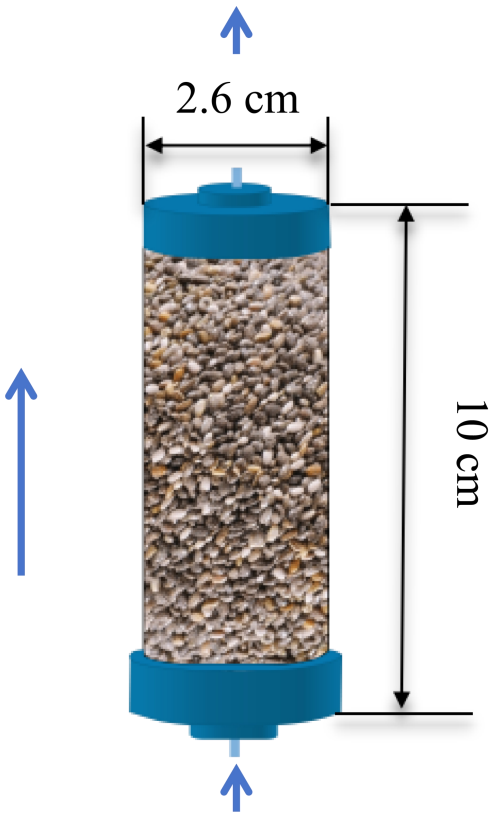

Figure. S2. Column Experiment Conceptual Model

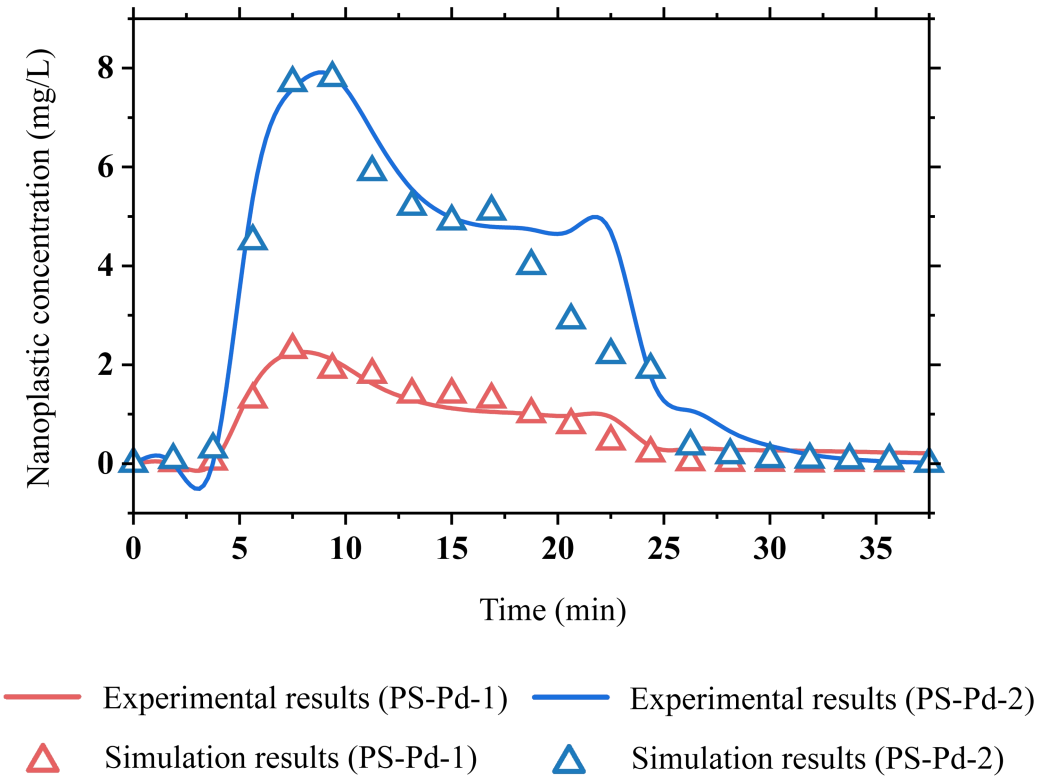

Figure. S3. Concentrations obtained through column experiments versus numerical simulation results approximated by adjusting nanoplastic migration parameters

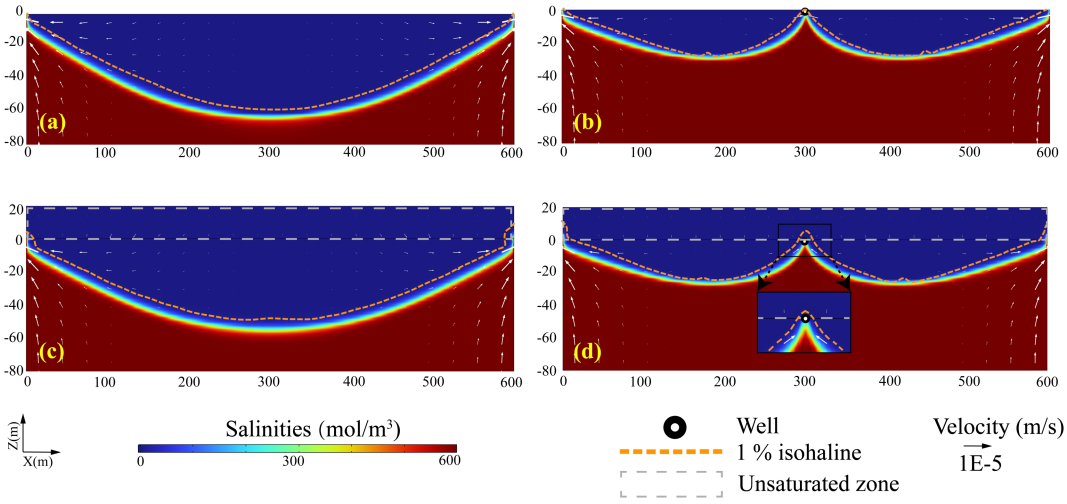

Figure. S4. Simulation results for freshwater lens formation and central-apex pumping in island aquifers: (a) and (b) respectively depict the freshwater lens formation stage and central-apex pumping conditions simulated within Tang et al.'s numerical reference scenario, with results extracted from the upper 80 m aquifer; (c) and (d) present scaled-up simulations of the freshwater lens formation stage and the freshwater lens under mid-top pumping conditions, respectively, incorporating an unsaturated zone added to Tang et al.'s reference control experiment setup. Results cover the 80 m saturated aquifer and the overlying 20 m unsaturated zone. The yellow dashed line denotes the 1% isohaline. The black-framed section, indicated by black arrowed dashed lines, represents an enlarged view of the wellhead vicinity. The black-edged white dot marks the extraction wellhead location at the uppermost 0 m of the saturated zone, precisely at the island's centre.

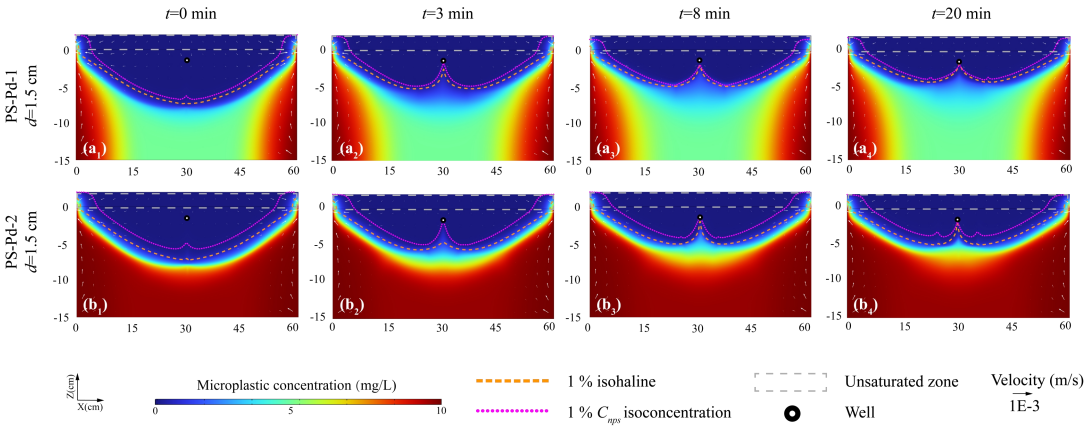

Figure. S5. Simulated nanoplastic concentrations in laboratory-scale idealized strip island aquifers during pumping: ($a_1/a_2/a_3/a_4$) Concentration distributions of hydrophilic nanoplastics (PS-Pd-1) and ($b_1/b_2/b_3/b_4$) hydrophobic nanoplastics (PS-Pd-2) at 0, 3, 8, and 20 minutes post-pumping. Orange dashed lines represent the 1% C_{nps} isoconcentration lines, pink dotted lines represent the 1% isohalinies, and gray shaded areas represent the unsaturated zone.

References

van Genuchten, M.T.: A Closed-form Equation for Predicting the Hydraulic Conductivity of Unsaturated Soils, Soil Science Society of America Journal, 44: 892-898, https://doi.org/10.2136/sssaj1980.03615995004400050002x, 1980.